Design of a Trap-Assisted Exceptional-Surface-Enhanced Silicon-on-Insulator Particle Sensor

Martino De Carlo, Francesco De Leonardis, *Member, IEEE*, Richard A. Soref, *Life Fellow, IEEE*, and Vittorio M. N. Passaro, *Senior Member, IEEE*

***Abstract*—Due to the recent interest in nanoparticles for both new functionalities and health-and-environment risks-related particle emissions of vehicles and industries, integrated-photonic single-particle sensors are urgently required. Exceptional surfaces (ESs) have been demonstrated to enhance the sensitivity of optical sensors and particle sensing is one of the most promising applications of ESs. The aim of this work is to show an ES-based architecture suitable for sensing the presence of nanoparticles with the aid of particle trapping allowed by optical forces. The solution proposed here enables the particle sensing with a passive architecture on an SOI chip. In this work it is shown that an SOI slot-waveguide-based ring-resonator architecture can be used for sub-50 nm single-particle sensing. Moreover, with a thermo-optic modulator we demonstrate that it is possible to measure the size of the particle, independently of its position along the ring resonator, with robustness to parameter fluctuations and noise.**

***Index Terms*—Exceptional point, exceptional surface, non-hermitian photonics, particle sensor, silicon on insulator, slot waveguides.**

I. Introduction

THE possibility of detecting and sizing single nanoparticles, with high resolution is essential to understand the behavior of particles and their size-dependent properties in order to develop new functionalities and new products [1]. With the recent advances in nanotechnology, different sizes and different materials have been used to synthesize nanoparticles for several applications [2], [3]. At the same time, nanoparticles generated by vehicles and industry have become sources of potential hazards for health and the environment [4], [5].

Although microscopy and spectroscopy have been used for single nanoparticle detection, their expensive and bulky instrumentation, together with the long processing times and the need for labelling, have prevented their widespread use [1]. The miniaturization of label-free particle sensing could represent a good alternative to microscopy and spectroscopy for the realization of compact and portable devices.

The integration of the photonic devices for particle sensing has been widely investigated in literature with microtoroids in Silica. Silica microtoroids are particularly useful for particle sensing, thanks to the low refractive index contrast between silica and air: the strong light–matter interactions in whispering-gallery-mode (WGM) microresonators [6], [7] can be used for ultrasensitive optical detection. The detection of the influenza virus and other biomolecules has been demonstrated in [8]–[11] using the frequency shift of a WGM due to the presence of targets onto the resonator surface and in [1] the mode splitting into of a WGM in a Silica microtoroid has been used to detect particles. Moreover, recently, Silica microtoroids have been used together with the architectures of non-Hermitian photonics to enhance the sensitivity of particle sensors [12], [13]. In this context, the first exceptional-surface-(ES) enhanced single-particle sensor was proposed in [14]. In [15], the first experimental validation of an ES-enhanced particle sensor has been published.

Differently from Silica, due to the high refractive index contrast of Silicon with air and to the consequent high confinement of light in Silicon cores, Silicon-On-Insulator (SOI) integrated strip or rib waveguides are not well suited for particle sensing. However, slot waveguides can be designed in SOI for enhancing the interaction of light with particles [16], [17]. In particular, in [18] an SOI slot-waveguide-based gold particle-sensing principle is proposed, simultaneously exploiting the optical trapping enhanced by optical resonance.

In a similar way, in this work we exploit the concept of slot waveguides arranged as an optical resonator both for trapping and for sensing and we simultaneously implement the concept of ESs of non-Hermitian photonics for enhancing the nanoparticle sensitivity. The advantages of the proposed solution would enable sensing of sub-50-nm particles with integrated SOI waveguides. This solution would make possible the realization of a fully integrated version of particle sensing, with laser bonding and direct excitation of the sensing region, without the need of external microfibers (as instead needed in Silica microtoroids). In this perspective, the complete miniaturization of the particle sensor could be achieved via a full integration. Moreover, with respect to the solution proposed in [14], the trap-assisted sensing enhanced by slot waveguides in this work will enable the trapping of particles for air monitoring applications.

Manuscript received 18 January 2022; revised 12 April 2022 and 24 May 2022; accepted 20 June 2022. Date of publication 23 June 2022; date of current version 2 September 2022. The work of R. A. Soref was supported by the Air Force Office of Scientific Research under Grant FA9550-21-1-0347. *(Corresponding author: Martino De Carlo.)*

Martino De Carlo, Francesco De Leonardis, and Vittorio M. N. Passaro are with the Photonics Research Group, Department of Electrical and Information Engineering, Politecnico di Bari, 70126 Bari, Italy (e-mail: martino.decarlo@poliba.it; francesco.deleonardis@poliba.it; vittorio.passaro@poliba.it).

Richard A. Soref is with the University of Massachusetts, Boston, MA 01003-9301 USA (e-mail: soref@rcn.com).

Color versions of one or more figures in this article are available at https://doi.org/10.1109/JLT.2022.3185829.

Digital Object Identifier 10.1109/JLT.2022.3185829

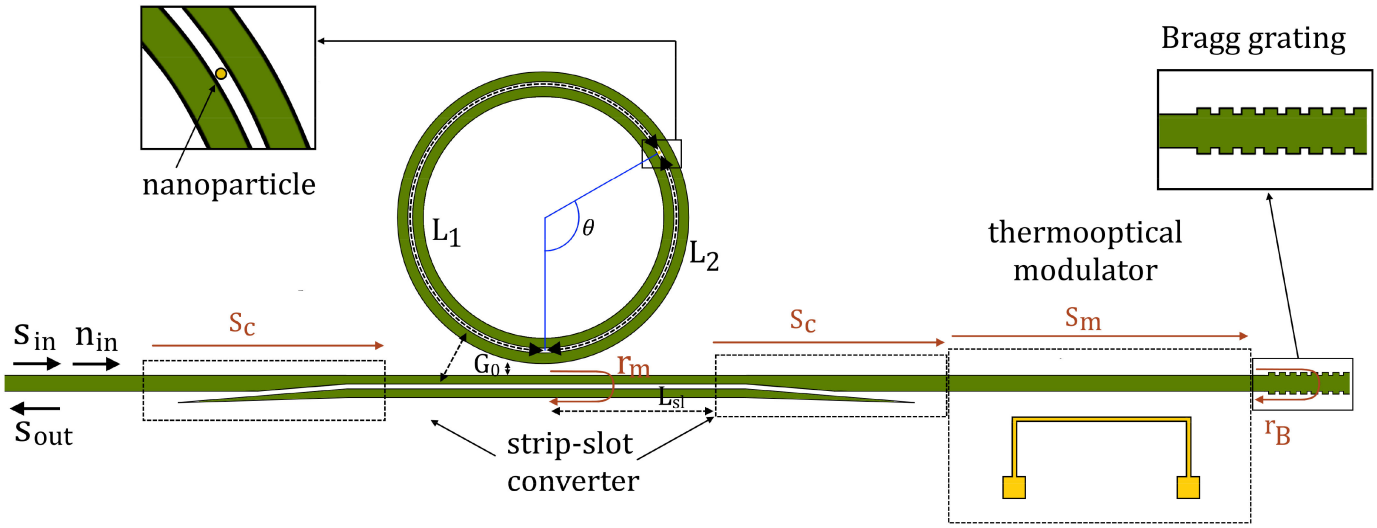

Fig. 1. Architecture of the ES particle sensor in the SOI platform, comprised of a ring resonator (realized with slot waveguides), two strip-slot converters, a Bragg grating reflector and a thermo-optical modulator.

Finally, the use of a simple thermo-optic modulator will enable a position-independent reading of the output.

II. Exceptional-Surface-Enhanced Particle Sensor

In this section the design of a nanoparticle sensor designed in SOI will be shown, with focus on the ES-based sensing and on the trapping mechanism. The basic idea is to design an optical resonator based on slot-waveguides to enhance both nanoparticle trapping and sensing. The full device proposed here is sketched in Fig. 1. In particular, the architecture includes a ring resonator realized with a slot waveguide, and its feeding bus, realized via a strip SOI waveguide, directly coupled into a slot waveguide only in the proximity of the coupling region with the resonator, in order to improve the coupling efficiency of the feeding bus with the ring. A Bragg grating is present at the end of the feeding bus, as is necessary in the ES-based architecture.

As for the optical architecture, we will design a device based on the concept of the ES that is a more robust way for implementing an exceptional point (EP). The strong spectral response of EPs of non-Hermitian Hamiltonians has been widely studied, not only for various kinds of sensing [19]–[24], but also for other applications as lasing [25], optomechanics [26], [27], non-reciprocal transmission [28], [29] and others [30]–[32]. However, due to the extraordinary sensitivity exhibited by EPs and to the highly critical design conditions required by EPs, even small unwanted external perturbations heavily influence the EP condition. This is the reason why some recent research works [33], [34] have pointed out the non-extraordinary performance of EP-based sensors. In particular, the high sensitivity of EPs to several different design parameters increases at the same time both the signal (eigenfrequency splitting) and the noise, leading to an intrinsic bound on the signal-to-noise ratio [33]. Moreover, the usual need for gain and loss for setting an EP, makes the influence of noise unavoidable. To overcome this limitation, the concept of ES has been introduced in optics [14], a technique that exploits the unidirectional coupling between two counterpropagating

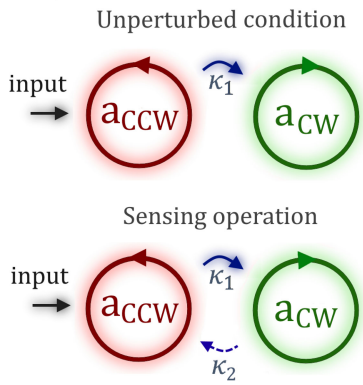

Fig. 2. Exceptional surface-based configuration illustrating schematically two waveguided modes within one microring resonator.

modes in the same cavity to make the system immune to all the sources of noise. By coupling two counterpropagating optical modes in a single resonant cavity, it is possible to make the sensor immune to all the differential perturbations that could affect two distinct cavities; and it is possible to combine robustness with the well-known high sensitivity of EPs for sensing applications [35]. The principle behind the ES is shown in Fig. 2: at the rest condition, only the counterclockwise (CCW) mode is coupled to the clockwise (CW) mode (with coupling strength κ_1). In this case, the perturbation to be sensed is represented by the coupling strength κ_2 between the CW and the CCW modes. It is easy to demonstrate that the eigenfrequency splitting between the eigenmodes of this system is proportional to $(\kappa_1\kappa_2)^{1/2}$ [35].

Since in this case κ_2 represents the perturbation to be sensed, the optimal sensitivity of the sensor is obtained when $\kappa_2 = 0$ (ES condition). So, the system should be designed to have κ_2 null in the unperturbed condition.

As demonstrated in [14], the only requirement for setting an ES-based sensor is the unidirectional coupling between the two counterpropagating modes in a single cavity: the absence of

critical design conditions makes ES-based signal robust versus the influence of noise, with respect to EP-based sensors: this is in perfect agreement with [33], where nonreciprocity is seen as a good solution to overcome the bounds in the signal-to-noise ratio and to enhance the sensitivity of mode-splitting type sensors.

This conceptual design can be implemented with the architecture in Fig. 1, using a Bragg grating reflector at the end of the feeding bus. Although the use of Bragg gratings has been widely investigated to couple counterpropagating modes (CW and CCWs) in optical resonators [36], [37], in this new configuration, the Bragg grating is used to realize the unidirectional coupling only between the CW and the CCW mode (κ_2) for the enhanced sensitivity at the ES.

The structure in Fig. 1 could be efficiently used to detect nanoparticles: as soon as a target particle interacts with the field inside the optical resonator, the backscattered fraction of CW and CCW propagating modes leads to $\kappa_2 \neq 0$ [14]. The generated splitting between the eigenfrequencies is proportional to $\kappa_2^{1/2}$ and can be related to the size of the particle [14].

In order to obtain an easy and robust model of the interaction of the particle with the optical architecture, the Scattering Matrix Method (SMM) is used here to design the device. The bus-ring directional coupler and the particle can be modelled with their scattering matrices as:

$$S_k = \begin{bmatrix} t & jk \\ jk & t \end{bmatrix} \tag{1a}$$

$$S_p = \begin{bmatrix} t_p & jr_p \\ jr_p & r_p \end{bmatrix} \tag{1b}$$

where t and jk are the transmission and coupling normalized amplitudes of the directional coupler, while t_p and jr_p are the transmission and reflection normalized amplitudes due to the particle backscattering.

The light is inputted from the input bus (s_{in}) and the output can be read from the same bus (s_{out}) with the aid of an optical circulator (either integrated or external). Physically s_{out} is the coherent optical interference between the optical signal reflected by the Bragg waveguide segment and the clockwise optical signal exiting the ring. The transfer function of the designed system, $s_{\text{out}}/s_{\text{in}}$, can be found to be:

$$\frac{s_{\text{out}}}{s_{\text{in}}} = S_c^2 \, \frac{r_m t^2 \; - j e^{2j\phi_1} k^2 r_p \; + \; e^{2j\phi} \, r_m - \; 2e^{j\phi} r_m t t_p}{e^{2j\phi} t^2 \; - \; 2e^{j\phi} t t_p \; + j e^{2j\phi_2} k^2 r_m r_p \; + \; 1} \tag{2}$$

where S_C is the transmitted amplitude (reciprocal) of the strip-slot converter, $\phi_{12} = \frac{2\pi}{\lambda} \, n_{\text{sl}} L_{12}$ (with L_1 and L_2 shown in Fig. 1, n_{sl} the effective index of all slotted waveguides, λ the operating wavelength), ϕ is equal to $\phi_1 + \phi_2$ and r_m is calculated as:

$$r_m = e^{j\phi_{sl}} \, S_C S_m r_B S_m S_C e^{j\phi_{sl}} \tag{3}$$

where $\phi_{\text{sl}} = (2\pi/\lambda) \, n_{\text{sl}} L_{\text{sl}}$ (with L_{sl} shown in Fig. 1), S_m is the reciprocal transmitted amplitude of the thermo-optic modulator in Fig. 1 and r_B is the Bragg grating reflected amplitude.

The eigenvalues related to (2) can be found in an implicit form by setting the denominator equal to zero:

$$e^{j\phi_{ES}} = \frac{t_p}{t} \; \pm \; j \frac{\sqrt{r_p^2 + jk^2 r_m e^{j(2\phi_2)} r_p}}{t}. \tag{4}$$

The eigenvalues splitting for very small values of r_p ($r_p \ll |k^2 r_m|$) is equal to

$$\Delta\phi_{ES} \approx 2\sqrt{jk^2 r_m e^{j(2\phi_2)} r_p} \tag{5}$$

and is proportional to the square root of the particle amplitude reflection ($r_p^{1/2}$), representing the advantage of the architecture [14]. It is immediately clear that the great advantage of this architecture is that the only condition required by this system to exhibit an enhanced sensitivity to small perturbations (square root dependance on r_p) is that the $r_p \ll |k^2 r_m|$. It is immediate to verify that this condition is not critical and is immediately realizable for very small particles (target of this sensor), with respect to the very critical design conditions required by EP-based sensors [33]. The absence of critical requirements makes ES-based configuration immune to the sources of noise that limits the signal-to-noise ratio in EP-based sensors. This has been possible because of the use of unidirectional coupling as the key element for sensing [33], as also in [14], [15] and [38].

It is immediately clear from Eq. (5) that a limitation of this architecture is that the eigenfrequency splitting is dependent on ϕ_2, which is related to L_2. Defining θ as the angular location of the airborne nanoparticle (having a chemical or biological nature) along the optical resonator, ($\theta \; = \; 2\pi L_2/(L_1 + L_2)$), ϕ_2 can be expressed as a function of θ. Consequently, the phase of the splitting is highly dependent on the position of the particle along the ring, making the readout quite difficult. In the next section the results of numerical simulations about the nanoparticle trapping and sensing will be shown and a method to solve the problem of the position-dependent reading will be proposed.

III. Numerical Results

In this section the results of numerical simulations about trapping and sensing of the particle will be shown and a proposal to solve the problem of the position-dependent reading will be developed. In particular, the simulations for the design will follow this process:

1) numerical simulations for characterizing the optical forces for particle trapping;
2) numerical evaluation of the amplitude reflection of the trapped nanoparticles inside the ring resonator;
3) design and simulations of the slot-slot directional coupler to feed the resonator and of the strip-to-slot waveguide converter;
4) numerical results about the implemented ES model, to sense the nanoparticle;
5) numerical simulations of a thermo-optic modulator to make the particle sensing more robust;
6) analysis of the effects of parameter fluctuations and noise.

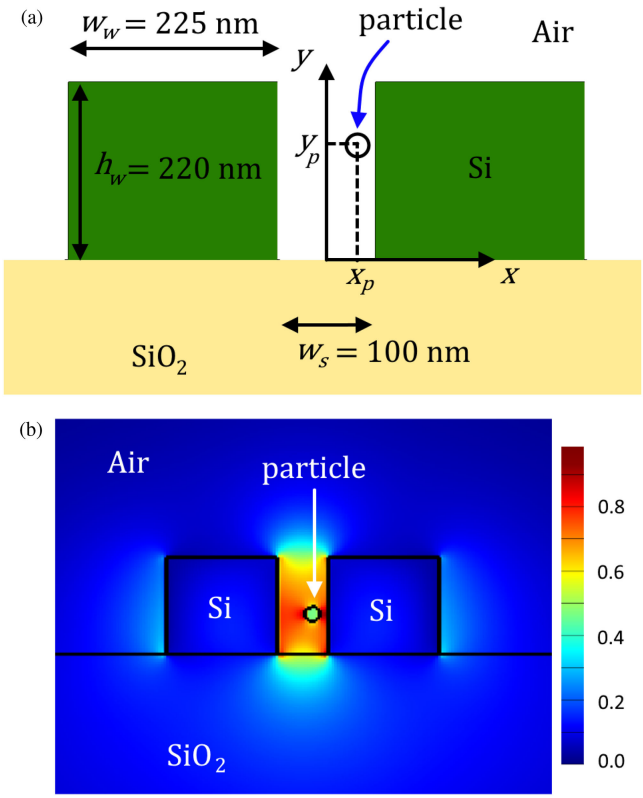

Fig. 3. (a) Schematic of the slot waveguide, indicating the sizes of the Silicon wires (w_w) and of the slot (w_s) and the coordinate reference system (b) Normalized Ex component of the electric field of the TE_0 mode of an SOI slot waveguide in the presence of a 15-nm particle placed at the vertical position corresponding to the potential well.

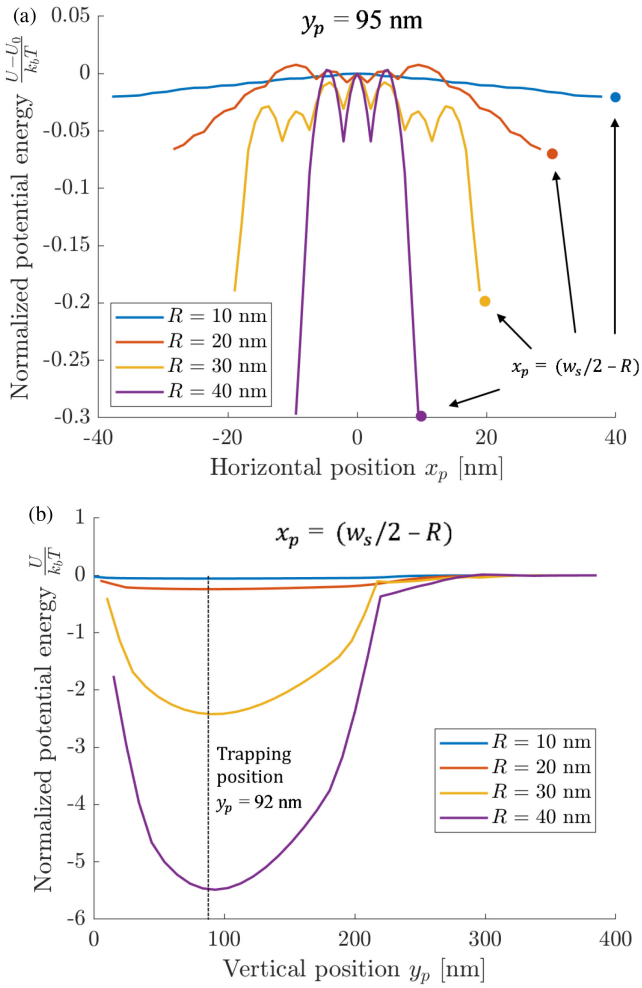

Fig. 4. (a) Normalized potential energy U (referenced to the potential energy, U_0, in $x_p = 0$) as a function of the horizontal position x_p, for $y_p = 95$ nm (for input power in the cross sections of the ring resonator of 1 mW). (b) Normalized potential energy as a function of the vertical position of the particle in the slot waveguide, for an incident power of 1 mW, for $x_p = \pm (w_s/2 - R)$ (corresponding to the extreme lateral position for a particle with radius R).

A. *Nanoparticle Trapping*

In order to improve the nanoparticle detection, optical forces have been exploited to attract the target particle in the proximity of the ring resonator. With this aim, a slot waveguide-based resonator has been designed for the ES architecture. Optical gradient forces and radiation pressure are the two well-known ways in which light exerts forces. In particular, optical field gradients caused by the evanescent fields of waveguides have been shown to allow the trapping of small particles [39], [40]. Slot waveguides represent a better choice than rib or strip waveguides for particle trapping [39], thanks to the high confinement of light in the covering medium (air in this example, for airborne particle trapping). In our design we have chosen a standard SOI wafer with 220-nm thick Silicon layer and 2-μm thick buried SiO_2. Air has been considered as the cover medium. The cross section of the designed strip waveguides has a width w_w of each Silicon arm of 225 nm and a slot width, w_s, of 100 nm (Fig. 3(a)). This cross section has been used to evaluate the optical force exerted on a nanoparticle of different sizes, to evaluate the trapping position and the necessary power to trap it. The Maxwell stress tensor [41] has been used to calculate the optical forces on a spherical nanoparticle with refractive index of 1.5 when varying the vertical position (y_p) and the horizontal position (x_p) of its center (Fig. 3(a)). Several particle radii R were investigated.

Initially, the horizontal position was set considering the particle placed in the middle of the slot ($x_p = 0$): the potential energy (associated with optical forces) has been calculated as a function of the vertical position y_p and a potential well has been calculated at $y_p = 95$ nm. Then, fixing the vertical position $y_p = 95$ nm, the potential energy has been calculated while varying the horizontal position x_p. It has been demonstrated that for all the particle sizes, there are two horizontal potential wells (in $x_p = \pm (w_s/2 - R)$) that push the particle towards the edges of the slot. In particular, the results of the potential energy U (referenced to the potential energy U_0, evaluated in $x_p = 0$, and normalized by k_BT, with k_B the Boltzmann constant and T the environmental temperature) are shown in Fig. 4(a) as a function of the horizontal position x_p, for the fixed value $y_p = 95$ nm (for input power in the cross sections of the ring resonator of 1 mW). As an example, for the particle with radius $R = 30$ nm, the potential well is in the position $x_p = \pm 20$ nm (for which the surface of the particle is in contact with the edge of the slot).

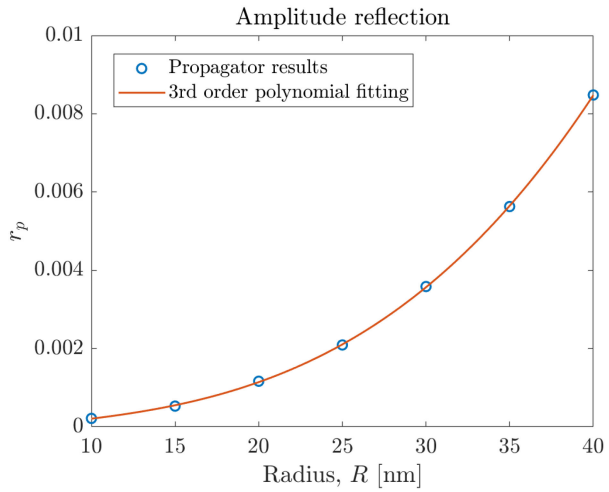

Fig. 5. Amplitude reflection coefficient, r_p, as a function of the radius of the particle, when the particle is trapped at the potential well.

Finally, fixing the horizontal position $x_p = w_s\ /2 - R$, the normalized potential energy (referenced to a position $y_p = +\infty$) has been calculated by varying the vertical position, y_p. The results in Fig. 4(b) show that there is a potential well at $y_p = 92$ nm. So, we can conclude that the trapping position for the particle will be at $x_p = \pm(w_s/2 - R)$ and $y_p = 92$ nm.

Thanks to the optical enhancement of optical resonators, it is possible to strengthen the potential well [18]. In this work the reflection induced by the interaction between the particle and the optical mode of the slot waveguide is used as the source for sensing. For this reason, the amplitude reflection r_p induced by a particle of a radius R has been calculated, when the particle is placed exactly at the vertical position $y_p = 92$ nm, corresponding to a potential well.

In this analysis we have neglected the effect of optical forces along the longitudinal coordinate of the ring resonator. A brief consideration about this will be found in section III.E.

B. Amplitude Reflection of Trapped Nanoparticle

Once the particle has been trapped inside the slot of the waveguide of the ring resonator, the amplitude reflection of the trapped particle (r_p) allows the exceptional surface sensing according to (2). In this context, the slot waveguide is useful, not only for enhancing particle trapping, but also for increasing the particle reflection. Fig. 5 shows the amplitude reflection of light in a slotted waveguide due to the presence of a nanoparticle of refractive index 1.5 trapped at the potential well (according to the simulations in Fig. 4(b)).

C. Slot-Slot Directional Coupler and Strip-Slot Direct Coupler

To feed the optical ring resonator, a bus-ring optical directional coupler is needed. Due to the high difference in propagation constants of light between a slot waveguide and a strip waveguide, coupling light with a strip waveguide bus to a slot-waveguide-based ring resonator would be not efficient. Thus, we designed a slot-slot directional coupler. Hence, we

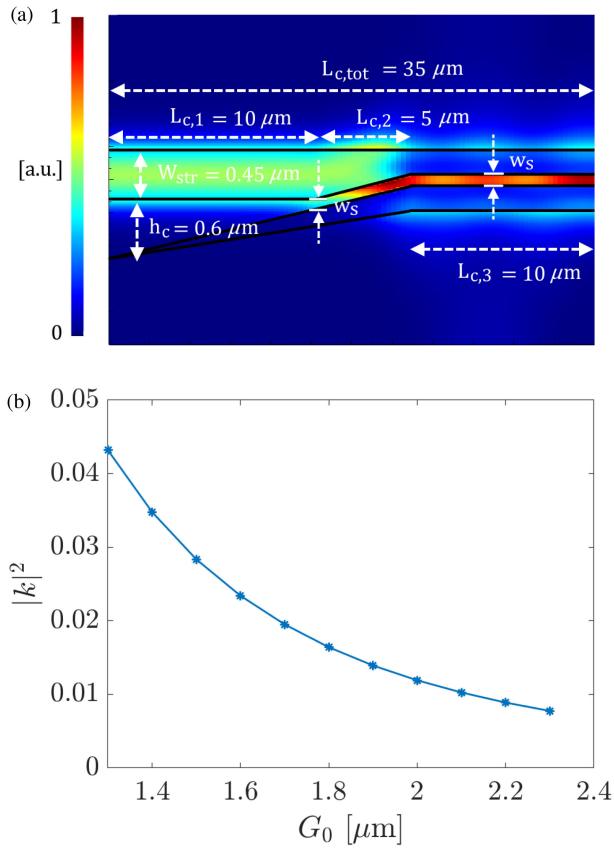

Fig. 6. (a) Transverse electric field in the strip-slot converter, with indication of the dimensions of the device. (b) Coupled power fraction between the slot waveguides of the directional coupler, as a function of the gap G_0 between the edges of the Silicon wires composing the slot waveguide (numerical results have been obtained with FDTD, with a ring resonator with a circumference of 100 μm).

also needed two identical strip-to-slot waveguide converters to be used before and after the coupling region.

As for the strip-to-slot converter, Fig. 6(a) shows the electric field in the strip-slot mode converter, (in particular with $L_{c1} = 10\,\mu$m, $L_{c2} = 5\,\mu$m, $L_{c3} = 10\,\mu$m, $h_c = 0.6\ \mu$m, $w_{str} = 0.45\ \mu$m). Using a propagator software, a direct power coupling efficiency of 91.2% has been numerically calculated at a wavelength of 1.55 μm, with a return loss lower than -65 dB.

Dealing with the bus-to-ring directional coupler, FDTD simulations have been used to evaluate the coupling ratio ($|k|^2$) as a function of the gap G_0 between the adjacent edges of the slotted waveguides of the bus and of the ring resonator (Fig. 6(b)).

D. Numerical Results of the ES-Enhanced Sensor

The model of the ES-enhanced particle sensor has been numerically implemented, using the results of the previous paragraphs. For the simulations, the width of the strip waveguides is $w_{str} = 450$ nm. An effective index of the slot waveguides of $n_{sl} = 1.4244$ and an effective index of the strip waveguides $n_{st} = 2.2730$ have been numerically calculated. The total length L of the circumference of the resonator has been set to 100 μm, leading to a central resonant wavelength $\lambda_0 = 1548.24$ nm. The length L_{sl} in Fig. 1 is equal to 20 μm and a propagation

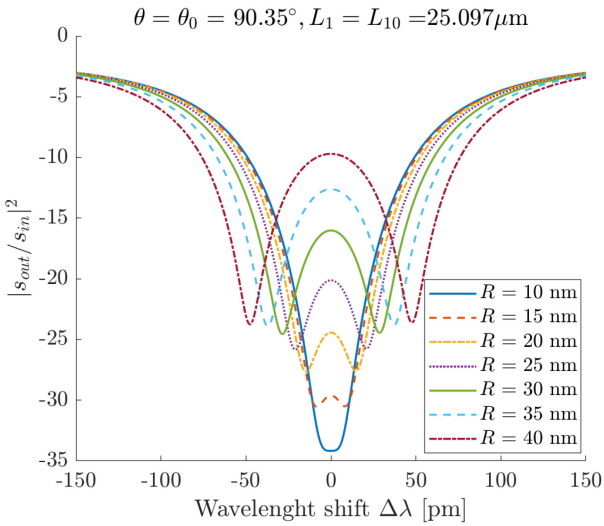

Fig. 7. Transfer function $|s_{\text{out}}/s_{\text{in}}|^2$ as a function of the wavelength, for different values of the radius of the trapped particle, at an angular position $L_1 = L_{10} = 25.097$ μm (corresponding to $\theta = \theta_0 = 90.35°$) along the resonator.

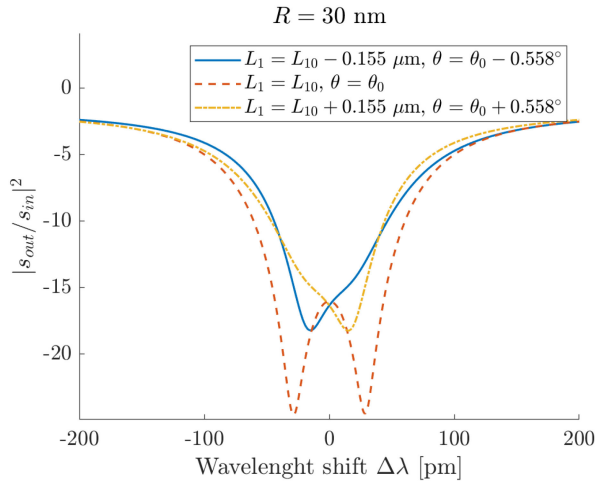

Fig. 8. Transfer function $|s_{out}/s_{in}|^2$ as a function of the wavelength shift (with respect to the central resonant wavelength, λ_0) for three values of the position of the trapped particle (of radius 30 nm) along the ring resonator.

loss of 9 dB/cm has been considered for slot waveguides, for a conservative design. A value of k of the slot-slot directional coupler of 0.16 ($|k|^2$= 2.56%) has been chosen, leading to a gap G_0 between the adjacent edges of the slot waveguides of 1555 nm (according to simulations Fig. 6(b)).

For the Bragg grating, the same model used in [35] has been adopted. In particular, the Bragg grating has been realized with a periodic structure made by 450-nm wide and 480-nm wide strip cross-sections, obtaining a grating coupling coefficient $\kappa = 1.8741 \cdot 10^5 \text{m}^{-1}$, with a duty cycle of 50%.

Fig. 7 shows the transfer function $|s_{out}/s_{in}|^2$ as a function of the wavelength shift with respect to the resonance wavelength, λ_0, of the isolated optical resonator for different sizes of the particle. The particle has been simulated to be trapped at an angular position $\theta_0 \approx 90.35°$, corresponding to a value of L_1 equal to 25.097 μm (because this position maximizes the sensitivity).

It is possible to appreciate that the splitting increases with the radius of the particle, due to an increased backscattered amplitude (Fig. 7). In particular, for a nanoparticle with radius R = 20 nm, a splitting $\Delta\lambda$ = 29 pm has been obtained, with a sensitivity $d(\Delta\lambda)/dR$ = 2.4 pm/nm.

This sensor chip utilizes a spectroscopic readout where the readout is triggered by a coherent input light source, such as a laser diode that has an emission linewidth of 200 pm to excite the spectrum in the wavelength region of interest. At the input/output edge of the chip, an optical circulator is used to read the returned power $|s_{out}|^2$ and then an optical spectrometer with a resolution of 1 pm is employed to determine the splitting of the resonance spectrum that is seen in Fig. 7, thereby determining the radius of the nanoparticle. The spectrometer is not looking for the absorption lines that give the chemical "signature" of the particle. Alternatively, a tunable laser source can be used to scan the transfer function across the wavelengths of interest, in combination with a photodiode instead of the spectrometer.

A problem of the proposed architecture is that the spectrum is highly dependent on the position of the particle θ (and so on the longitudinal position L_1) along the resonator, due to the dependence of the eigenfrequency splitting on ϕ_2. Fig. 8 shows the transfer function $|s_{out}/s_{in}|^2$ versus the wavelength shift in the presence of a trapped nanoparticle with a radius of 30 nm for longitudinal positions L_1 (and the corresponding θ) around the position of the maximum sensitivity, L_{10} (for $\theta = \theta_0$). It is possible to appreciate that for an error on the angular of position of only 0.155 μm (1/10 of the operating wavelength and around 5.17 times higher than the particle radius) the splitting in the transfer function is not visible anymore. So, a way to make the splitting reading independent of the angular position is needed. For this purpose, in this work we exploited the dependence of the eigenvalues splitting on r_m (5), which in turns depends on S_m (3). The idea developed here is to use the thermo-optic modulator to change the phase of S_m and have a way to extract the size of the nanoparticle independently of its position.

E. Thermo-Optic Modulator for Position-Independent Reading

In order to extract the dimension of the particle in a position-independent way, we designed a thermo-optic modulator, to be realized via the deposition of a thin (50 nm) film of gold with two electrodes and a resistive connection between them as in Fig. 9 forming an electrical Joule heater strip. In particular the dimensions d_m = 0.9 μm, L_m= 20 μm, w_m = 200 nm, H_m= 5 μm have been used. By applying a voltage difference between the two squared electrodes, a temperature increase is induced in the gold resistor, due to the Joule effect, and in its proximity. The temperature around the gold resistor has been evaluated via a 3D simulation of the heat propagation, with the boundary conditions of a fixed environmental temperature (300 K) at 100 μm above the chip and 100 μm below the interface between the buried oxide layer and the Silicon substrate. Fig. 10 shows the temperature along the center of the cross-section of

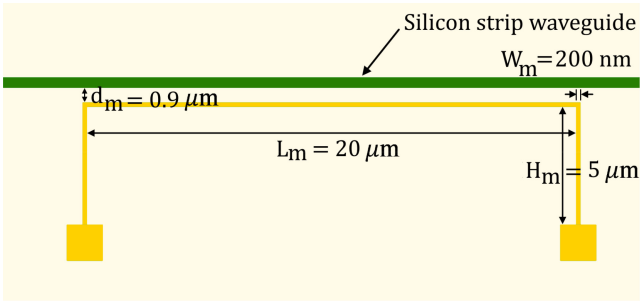

Fig. 9. Layout of the designed thermo-optic modulator, with two electrodes and a wire resistor of 50 nm-thick gold.

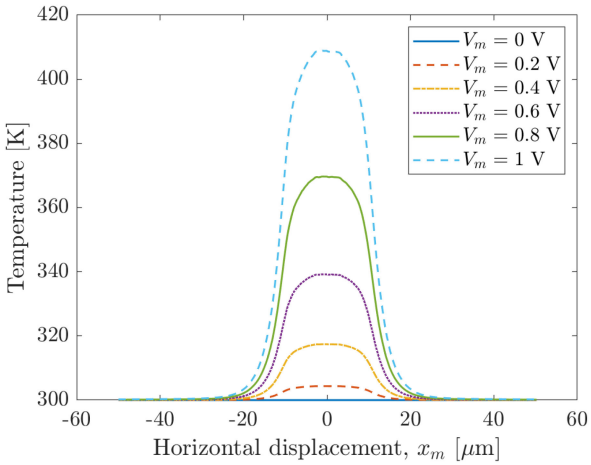

Fig. 10. Temperature as a function of the horizontal displacement along the thermo-optic modulator, for different values of the voltage difference applied at the gold electrodes.

the Silicon strip waveguide for several values of the voltage difference applied to the electrodes.

Using the thermo-optic coefficient of Silicon [42] and Silica [43], a value of $d_{n_{\text{eff}}}/dT = 2.2 \cdot 10^{-4}$ K^{-1} has been evaluated for the strip waveguide for different temperatures. These values have been useful to obtain the variation of S_m with temperature. In particular, the length of the simulated devices for the calculation of S_m is 100 μm (corresponding to the range plotted in the thermal simulations of Fig. 10).

In this way, the voltage difference across the electrodes could be used to finely tune the phase of the splitting during the operation of the sensor, in a feedback configuration. Another simpler solution that we propose in this work is to vary the voltage difference across all the values between 0 and 1 V and calculating the maximum difference between the wavelengths of all the resonance dips during all these measurements. This kind of approach has been simulated in Fig. 11, where a particle of $R = 30$ nm has been considered (at the longitudinal position $L_1 = L_{10} + 0.155$ μm). In this configuration, we need to estimate the dynamics of the thermo-optic modulator: we numerically simulated that the designed thermo-optic modulator has settling time (10% to 90%) of $t_r = 3$ μs, for an input step voltage of 1 V of amplitude.

In this analysis we have neglected the possible movement of the particle along θ during sensing since we guess that the

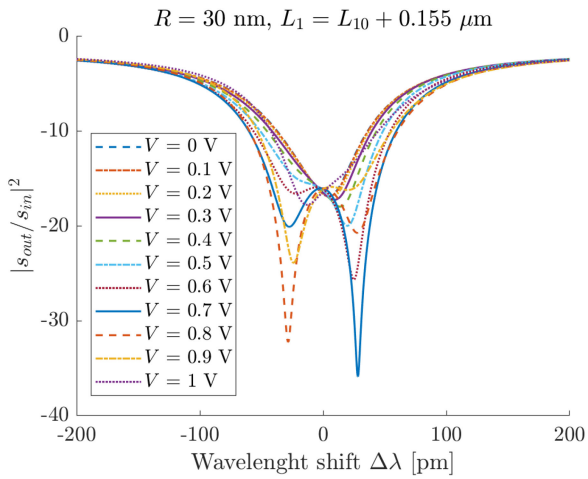

Fig. 11. Transfer function $|s_{out}/s_{in}|^2$ as a function of the wavelength, for different values of the applied voltage difference, at longitudinal position $L_1 = L_{10} + 0.155$ μm.

movement of the particle would make the term $e^{j\phi_2}$ in (5) change much slower than the phase variation we apply to r_m with the thermal tuning of S_m. In case this hypothesis was not verified, the thermal modulation would be useless, and the movement of the particle would be sufficient to obtain the effect in Fig. 11(see (5)).

Finally, with the design proposed here, we cannot in principle be sure about the presence of only one particle. So, we are required to track the particles during time, identifying any new particle as a discontinuity in measured eigenfrequency splitting, as in [1], with the difference that, in this design, the eigenfrequency splitting depends nonlinearly (square root dependence) on the particle reflection amplitude.

F. Robustness to Parameter Fluctuations and Noise

The design proposed in this paper exploits the concept of ES, that has been demonstrated to be much more robust than EPs to fluctuations of parameters [14]. However, we showed that the uncertainty on the particle positions (and in general any fluctuation in the phase of the radicand in (5)) can spoil the resolvability and the sensitivity (Fig. 8). We demonstrated that this problem can be solved by sweeping the temperature in the feeding bus with an electro-optic modulator and by reading the maximum difference ($\Delta\lambda_{max}$) between all the resonant dip wavelengths in the transfer function, during voltage-induced temperature changes (as in Fig. 11). A reader could complain about the immunity of ES to other parameters fluctuations that typically strongly affect EP-based sensors (i.e., resonance frequency of the resonators and loss in the resonators). Fig. 12(a) and (b) show the value of $\Delta\lambda_{max}$ (simulated with the sweep of the voltage between 0 V and 1 V with a step of 0.05 V) as a function of the effective index (n_{sl}) of the slot waveguides (composing the ring resonator and part of the feeding bus) and of the loss of the slot waveguides (α), respectively, for three values of the radius of the particle. So, it is immediate to notice that the readings aren't heavily affected by those parameters of the sensor, even for very high ranges of

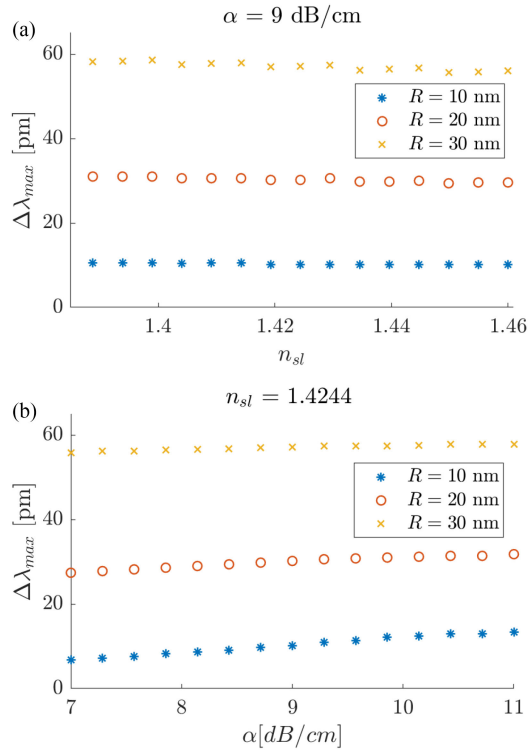

Fig. 12. Maximum difference ($\Delta\lambda_{max}$) between all the resonant dip wavelengths in the transfer function, during voltage-induced temperature sweep, as a function of the effective index of the slot waveguides (a) and of the loss of the slot waveguides (b), for three values of the radius of the particle.

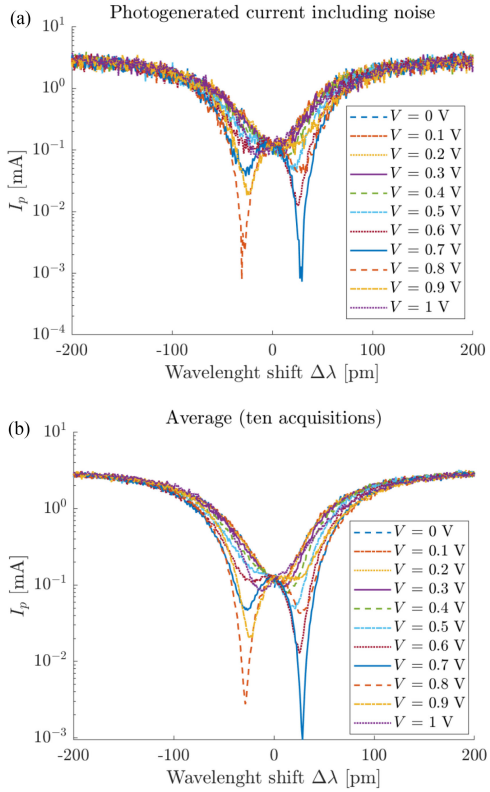

Fig. 13. Effect of noise on the photocurrent (a) and averaged photocurrent with ten simulated acquisitions (b), in the same conditions proposed in Fig. 11.

variations of the fluctuating parameters. Possible variations of the nondimensional coupling coefficient between the ring and the feeding bus wouldn't affect the ES design but would affect the sensitivity of the sensor according to (5). This demonstrates that ES is preserved, even with high fluctuations of the design parameters, thus confirming the superiority of ES with respect to EP, in accordance with [14].

We also included the main sources of noise that we consider would affect the performance of the fully passive photonic device proposed here. We investigated three sources of zero-mean gaussian intensity noise [44]:

1) Relative Intensity Noise (RIN) that has been considered to be injected in the system via the input bus (n_{in}, in Fig. 1).
2) Shot Noise (power spectral density of $S_{sh} = 2eI_{PD}$, with e the electron charge, and I_{PD} the photogenerated current) that affects the photogenerated current at the photodetector.
3) Johnson Noise (power spectral density of $S_J = 4k_BT_{PD}/R_L$, with k_B the Boltzmann constant, T_{PD} the temperature of the photodetector and R_L the load resistance of the detector) that also affects the photogenerated current at the photodetector.

For the noise analysis, we have considered the scan of a tunable laser source of 10 dBm with a scanning step of 1 pm, with a RIN of -130 dB/Hz and with a linewidth negligible with respect to the scanning step. Then, for the shot noise and the Johnson noise, we have considered a photoreceiver at a temperature of $T_{PD} = 300\ K$, with a responsivity of 0.5 A/W, a bandwidth of $B = 50$ GHz (corresponding to approximately 400 pm at 1.55 μm) and a load resistance of $R_L = 1\ k\Omega$. Fig. 13(a) shows the effect of the analyzed sources of noise on the photocurrent (in the same conditions considered in Fig. 11). Since all the noise sources have a zero mean, averaging several acquisitions leads to the reduction of the effect of noise: Fig. 13(b) shows the effect of averaging on ten different simulated acquisitions. It is easy to appreciate that the system is robust to the three classical sources of noise analyzed here.

IV. Conclusion

In conclusion, we have demonstrated that a high sensitivity sensor of airborne nanoparticles can be developed in the SOI platform for detecting the presence of a single nanoparticle with radii lower than 50 nm. In particular, for a nanoparticle of 20 nm (refractive index of 1.5), a splitting of 22.2 pm has been obtained, with a sensitivity with respect to the particle radius of 2.8 pm/nm. Using the ES-approach, we demonstrated that is possible to sense sub-50 nm particle using SOI waveguides, with the aid of particle trapping. Moreover, the proposed integrated photonic circuit is robust against fabrication errors thanks to the stable properties of the exceptional surface, and the splitting reading is independent of the position of the particle along the resonator, thanks to the use of a thermo-optic modulator. Finally, robustness to three sources of intensity noise has been demonstrated.

REFERENCES

[1] J. Zhu et al., "On-chip single nanoparticle detection and sizing by mode splitting in an ultrahigh-Q microresonator," *Nature Photon.*, vol. 4, no. 1, pp. 46–49, 2009, doi: 10.1038/nphoton.2009.237.

[2] B. O'Regan and M. Grätzel, "A low-cost, high-efficiency solar cell based on dye-sensitized colloidal TiO_2 films," *Nature*, vol. 353, no. 6346, pp. 737–740, 1991, doi: 10.1038/353737a0.

[3] P. Alivisatos, "The use of nanocrystals in biological detection," *Nature Biotechnol.*, vol. 22, no. 1, pp. 47–52, 2003, doi: 10.1038/nbt927.

[4] P. H. Hoet, I. Brüske-Hohlfeld, and O. V Salata,"Nanoparticles - known and unknown health risks", *J. Nanobiotechnology*, vol. 2, no. 1, 2004, Art. no. 12, doi: 10.1186/1477-3155-2-12.

[5] V. Colvin, "The potential environmental impact of engineered nanomaterials," *Nature Biotechnol.*, vol. 21, no. 10, pp. 1166–1170, 2003, doi: 10.1038/nbt875.

[6] K. Vahala, "Optical microcavities," *Nature*, vol. 424, no. 6950, pp. 839–846, 2003, doi: 10.1038/nature01939.

[7] D. Armani, T. Kippenberg, S. Spillane, and K. Vahala, "Ultra-high-Q toroid microcavity on a chip," *Nature*, vol. 421, no. 6926, pp. 925–928, 2003, doi: 10.1038/nature01371.

[8] F. Vollmer and S. Arnold, "Whispering-gallery-mode biosensing: Label-free detection down to single molecules," *Nature Methods*, vol. 5, no. 7, pp. 591–596, 2008, doi: 10.1038/nmeth.1221.

[9] A. Armani, R. Kulkarni, S. Fraser, R. Flagan, and K. Vahala, "Label-Free, single-molecule detection with optical microcavities," *Science*, vol. 317, no. 5839, pp. 783–787, 2007, doi: 10.1126/science.1145002.

[10] F. Vollmer, S. Arnold, and D. Keng, "Single virus detection from the reactive shift of a whispering-gallery mode," *Proc. Nature Acad. Sci.*, vol. 105, no. 52, pp. 20701–20704, 2008, doi: 10.1073/pnas.0808988106.

[11] I. White, H. Oveys, and X. Fan, "Liquid-core optical ring-resonator sensors," *Opt. Lett.*, vol. 31, no. 9, 2006, Art. no. 1319, doi: 10.1364/ol.31.001319.

[12] J. Wiersig, "Enhancing the sensitivity of frequency and energy splitting detection by using exceptional points: Application to microcavity sensors for single-particle detection," *Phys. Rev. Lett.*, vol. 112, no. 20, 2014, doi: 10.1103/physrevlett.112.203901.

[13] J. Xiao-Xue, Y. Gao, Z. Shi-Hui, T. Wang, and C. Wang, "The particle induced mode splitting and exceptional points in whispering-gallery mode microcavity," *IEEE Photon. J.*, vol. 12, no. 6, pp. 1–14, Dec. 2020, doi: 10.1109/jphot.2020.3030702.

[14] Q. Zhong, J. Ren, M. Khajavikhan, D. Christodoulides, Ş. Özdemir, and R. El-Ganainy, "Sensing with exceptional surfaces in order to combine sensitivity with robustness," *Phys. Rev. Lett.*, vol. 122, no. 15, 2019, Art. no. 153902, doi: 10.1103/physrevlett.122.153902.

[15] G. Qin et al., "Experimental realization of sensitivity enhancement and suppression with exceptional surfaces," *Laser Photon. Rev.*, vol. 15, no. 5, 2021, Art. no. 2000569, doi: 10.1002/lpor.202000569.

[16] C. A. Barrios, "Optical slot-waveguide based biochemical sensors," *Sensors*, vol. 9, no. 6, pp. 4751–4765, 2009, doi: 10.3390/s90604751.

[17] C. A. Barrios et al., "Slot-waveguide biochemical sensor," *Opt. Lett.*, vol. 32, no. 21, pp. 3080–3082, 2007, doi: 10.1364/ol.32.003080.

[18] J. Witzens and M. Hochberg, "Optical detection of target molecule induced aggregation of nanoparticles by means of high-Q resonators," *Opt. Exp.*, vol. 19, no. 8, pp. 7034–7061, 2011, doi: 10.1364/oe.19.007034.

[19] J. Ren et al., "Ultrasensitive micro-scale parity-time-symmetric ring laser gyroscope," *Opt. Lett.*, vol. 42, no. 8, pp. 1556–1559, 2017, doi: 10.1364/ol.42.001556.

[20] M. De Carlo, F. De Leonardis, and V. Passaro, "Design rules of a microscale PT-Symmetric optical gyroscope using group IV platform," *J. Lightw. Technol.*, vol. 36, no. 16, pp. 3261–3268, 2018, doi: 10.1109/jlt.2018.2837754.

[21] M. De Carlo, F. De Leonardis, L. Lamberti, and V. Passaro, "High-sensitivity real-splitting anti-PT-symmetric microscale optical gyroscope," *Opt. Lett.*, vol. 44, no. 16, pp. 3956–3959, 2019, doi: 10.1364/ol.44.003956.

[22] M. De Carlo, "Exceptional points of parity-time- and anti-parity-time-symmetric devices for refractive index and absorption-based sensing," *Results Opt.*, vol. 2, 2021, Art. no. 100052, doi: 10.1016/j.rio.2020.100052.

[23] W. Li et al., "Real frequency splitting indirectly coupled anti-parity-time symmetric nanoparticle sensor," *J. Appl. Phys.*, vol. 128, no. 13, 2020, Art. no. 134503, doi: 10.1063/5.0020944.

[24] J. Wiersig, "Review of exceptional point-based sensors," *Photon. Res.*, vol. 8, no. 9, 2020, Art. no. 1457, doi: 10.1364/prj.396115.

[25] M. Brandstetter et al., "Reversing the pump dependence of a laser at an exceptional point," *Nature Commun.*, vol. 5, no. 1, 2014, Art. no. 4034, doi: 10.1038/ncomms5034.

[26] W. Li, Y. Jiang, C. Li, and H. Song, "Parity-time-symmetry enhanced optomechanically-induced-transparency," *Sci. Rep.*, vol. 6, no. 1, 2016, Art. no. 31095, doi: 10.1038/srep31095.

[27] M. De Carlo, F. De Leonardis, L. Lamberti, and V. Passaro, "Generalized modeling of optomechanical forces applied to PT-Symmetric optical microscale resonators," *J. Lightw. Technol.*, vol. 37, no. 10, pp. 2178–2184, 2019, doi: 10.1109/jlt.2019.2899486.

[28] B. Peng et al., "Parity–time-symmetric whispering-gallery microcavities," *Nature Phys.*, vol. 10, no. 5, pp. 394–398, 2014, doi: 10.1038/nphys2927.

[29] X. Zhang, T. Jiang, and C. Chan, "Dynamically encircling an exceptional point in anti-parity-time symmetric systems: Asymmetric mode switching for symmetry-broken modes," *Light: Sci. Appl.*, vol. 8, no. 1, 2019, Art. no. 88, doi: 10.1038/s41377-019-0200-8.

[30] H. Benisty et al., "Implementation of PT symmetric devices using plasmonics: Principle and applications," *Opt. Exp.*, vol. 19, no. 19, pp. 18004–18019, 2011, doi: 10.1364/oe.19.018004.

[31] S. Zhang, Z. Yong, Y. Zhang, and S. He, "Parity-time symmetry breaking in coupled nanobeam cavities," *Sci. Rep.*, vol. 6, no. 1, 2016, Art. no. 24487, doi: 10.1038/srep24487.

[32] S. Klaiman, U. Günther, and N. Moiseyev, "Visualization of branch points in PT-Symmetric waveguides," *Phys. Rev. Lett.*, vol. 101, no. 8, 2008, Art. no. 080402, doi: 10.1103/physrevlett.101.080402.

[33] H. Lau and A. Clerk, "Fundamental limits and non-reciprocal approaches in non-Hermitian quantum sensing," *Nature Commun.*, vol. 9, no. 1, 2018, Art. no. 4320, doi: 10.1038/s41467-018-06477-7.

[34] W. Langbein, "No exceptional precision of exceptional-point sensors," *Phys. Rev. A*, vol. 98, no. 2, 2018, Art. no. 023805, doi: 10.1103/physreva.98.023805.

[35] M. De Carlo, F. De Leonardis, R. Soref, and V. Passaro, "Design of an exceptional-surface-enhanced silicon-on-insulator optical accelerometer," *J. Lightw. Technol.*, vol. 39, no. 18, pp. 5954–5961, 2021, doi: 10.1109/jlt.2021.3091333.

[36] C. Campanella, M. De Carlo, A. Cuccovillo, F. De Leonardis, and V. M. N. Passaro, "Methane gas photonic sensor based on resonant coupled cavities," *Sensors*, vol. 19, no. 23, 2019, Art. no. 5171, doi: 10.3390/s19235171.

[37] C. Campanella, M. De Carlo, A. Cuccovillo, and V. Passaro, "Loss-induced control of light propagation direction in passive linear coupled optical cavities," *Photon. Res.*, vol. 6, no. 6, 2018, Art. no. 525, doi: 10.1364/prj.6.000525.

[38] S. Jiang et al., "Enhanced nanoparticle sensing by mode intensity in a non-reciprocally coupled microcavity," *J. Appl. Phys.*, vol. 131, no. 10, 2022, Art. no. 103106, doi: 10.1063/5.0082364.

[39] A. Yang, S. Moore, B. Schmidt, M. Klug, M. Lipson, and D. Erickson, "Optical manipulation of nanoparticles and biomolecules in sub-wavelength slot waveguides," *Nature*, vol. 457, no. 7225, pp. 71–75, 2009, doi: 10.1038/nature07593.

[40] J. Hole, J. Wilkinson, K. Grujic, and O. Hellesø, "Velocity distribution of gold nanoparticles trapped on an optical waveguide," *Opt. Exp.*, vol. 13, no. 10, pp. 3896–3901, 2005, doi: 10.1364/opex.13.003896.

[41] D. Griffiths, *Introduction to Electrodynamics*. San Francisco, CA, USA: Pearson, 2008.

[42] J. Komma, C. Schwarz, G. Hofmann, D. Heinert, and R. Nawrodt, "Thermo-optic coefficient of silicon at 1550 nm and cryogenic temperatures," *Appl. Phys. Lett.*, vol. 101, no. 4, 2012, Art. no. 041905, doi: 10.1063/1.4738989.

[43] T. Toyoda and M. Yabe, "The temperature dependence of the refractive indices of fused silica and crystal quartz," *J. Phys. D: Appl. Phys.*, vol. 16, no. 5, pp. L97–L100, 1983, doi: 10.1088/0022-3727/16/5/002.

[44] X. Zhou, L. Zhang, and W. Pang, "Performance and noise analysis of optical microresonator-based biochemical sensors using intensity detection," *Opt. Exp.*, vol. 24, no. 16, pp. 18197–18208, 2016, doi: 10.1364/oe.24.018197.